Modification of interfacial tension by considering the effect of porous medium during near miscible gas injection

Hossein Mehrjoo [a], Yousef Kazemzadeh [b*], Ali Safaei [c], Masoud Riazi [c]**

[a] Department of Petroleum Engineering, Shahid Bahonar University of Kerman, Kerman, Iran
[b] Department of Petroleum Engineering, School of Chemical and Petroleum Eng. Shiraz University, Shiraz. Iran
[c] Enhanced Oil Recovery (EOR) Research Centre, IOR/EOR Research Institute, Shiraz University, Shiraz, Iran

Abstract: Gas injection as one of the interesting enhance oil recovery (EOR) methods has been attracted many attentions, hence, numerous experimental and simulation studies of this process were investigated by several researchers. However, an investigation of some parameters such as the effect of injection gas, the effect interfacial tension (IFT) at minimum miscible pressure (MMP), named IFT0 in the present study, the impact of porous medium on the IFT and subsequently on the gas injection process is still missing. Hence, in this paper, the effect of injection gases, IFT0, and the influence of porous media on the IFT and then on the fractional flow of gas, saturation curve of gas, and relative permeability of oil and gas were investigated. Depending on the type of injection gases used, our findings indicate that different MMPs can be achieved. Additionally, the type of injection gases affects fractional flow, saturation, and relative permeability curves. Our investigation illustrated that the impact of IFT0 aforementioned curves is depended on the miscible and immiscible conditions. The effect of porous medium and fracture on the IFT of system have observed, while modified IFT did not affect fractional flow, saturation, and relative permeability curves.

Keywords: Interfacial tension, Gas injection, Enhancing oil recovery, Minimum miscible pressure, Near miscible injection

*Corresponding author: yusefkazemzade@yahoo.com

**Corresponding author: mriazi180@gmail.com

1. Introduction

It is essential to increase crude oil production to meet the increasing energy demand in the world. Improved oil recovery techniques, including gas injection, are essential for enhancing oil production [1, 2]. In gas injection method, hydrocarbon gas (i.e., produced and natural gas) and non-hydrocarbon gas (i.e., carbon dioxide, nitrogen) are used [3, 4], and gas can be injected in near miscible, miscible, or immiscible conditions. The main mechanisms in gas injection are reduction in oil viscosity and or interfacial tension (IFT), dissolved gas drive, and volumetric gas injection [3, 4]. The extent to which each mechanism contributes depends on the conditions of the reservoir and fluid [5]. The primary mechanism of gas flooding is the reduction of the IFT and increasing the miscibility of the injection and reservoir fluid [6, 7].

Many researchers have investigated experimentally the effect of different factors on the gas injection process. Shariatpanahi et al. [8] carried out two sets of experiments to investigate the behavior of immiscible and water flooding. The researchers conducted their experiments using two-dimensional porous micromodels with fractures. According to their findings, the maximum oil recovery achieved through immiscible gas injection was 60%. Their oil recovery after water flooding was more than the recovery of immiscible gas injection, and it was about 75%. In 2005, Dastyari et al. [9] carried out an experiment to investigate the immiscible gas injection in a micromodel under the influence of gravity. Their results showed that residual oil saturation in case of natural depletion and in a situation that flow was aligned with gravity was lower than gas injection in different angles. Nematzadeh et al. [10] conducted an experimental study of secondary WAG injection in carbonate cores at low temperature and different pressure conditions. Based on their results, before minimum miscible pressure (MMP), enhancing the oil recover was observed by increasing the pressure. They showed that miscible WAG resulted in higher oil recovery. In 2012, Motealleh et al. [11] investigated the performance of WAG in one of Iranian reservoir. Their experimental investigation showed that secondary miscible WAG injection resulted in the highest oil recovery. Yu et al. [12] studied experimentally the efficiencies of nitrogen huff-n-puff and its flooding in shale samples. The findings suggest that the effectiveness of N_2 huff-n-puff was superior to that of N_2 flooding. Although both methods had similar efficiency before a breakthrough, after breakthrough production rate by gas flooding was reduced.

Fahandezhsaadi et al. [13] studied N_2 injection for enhanced oil recovery (EOR) and investigated the effects of induced fractures and pressure. They displayed gas breakthrough and onset time of oil production were related to differential pressures and induced fractures. Wang et al. [14] developed representative micromodel to study the EOR mechanism of the injection of the immiscible CO_2 WAG at microscale. They showed injection of WAG after continuous CO_2 injection could influence both carbon dioxide capture storage and oil recovery. Li et al. [15] investigated the effectiveness of different injection strategies, including WAG, cyclic gas, and continuous gas injection, for CO2 storage and EOR in ultra-low permeability samples. The performance of WAG in both EOR and storage was better than continuous gas injection. The best injection scenario for storage and EOR was cyclic CO_2 injection. Mahzari et al. [16] introduced a novel laboratory approach to study the efficiency of huff-n-puff gas injection in shale oils. Two type of experiments were conducted in a study that in a first one the core was saturated with moveable oil and in a second one the core was saturated with associated gas and dead oil injection was injected in both experiments. Based on their experiments, more oil production was achieved in core that saturated with the live oil. Gandomkar and Sharif [17] examined the efficacy of nanocomposites as direct thickeners for gas injection to address the primary operational/technical challenge associated with gas injection, namely the low viscosity of the gas. Their findings indicated that the P-1-D nanocomposite, consisting of graphene oxide, could substantially enhance the viscosity of the gas. Reduction of IFT as result of utilize gas thickeners was another results of this study. Pore-scale mechanisms of miscible and immiscible gas injection in fractured carbonated was investigated by Chen and Mohanty [18]. Their findings indicated that the vugs were fully depleted after miscible gas injection, whereas they remained fully saturated with oil after immiscible gas injection. According to their findings, the ultimate oil recovery during immiscible injection in the matrix was affected by the permeability contrast between the fracture and matrix. During miscible injection, oil recovery was determined by diffusion in the early stages and miscible displacement in the later stages of injection. Zhao et al. [19] studied the impact of citric acid isopentyl ester and citric acid isobutyl ester on dropping the MMP of crude oil and CO_2. Based on their results optimum injected slug size of chemical reagents resulted in reduction of MMP [19]. In addition, more oil recovery was achieved as result of adding citric acid isobutyl ester [19].

Simulation of gas injection is another interesting study for most of the researchers. In 2002, Uleberg et al. [20] simulated gas injection in a fractured reservoir. Their simulation was based on compositional reservoir modeling. They developed a method for predicting of MMP and minimum miscibility enrichment (MME) in fractured media. They showed the MMP and MME in the fracture reservoir were higher than in a conventional single-porosity reservoir [20]. Vicencio et al. [21] simulated the injection of nitrogen in a naturally fractured reservoir, and they showed injected fluid, nitrogen, moved straight to the oil-gas contact. The main reason for this phenomenon was destabilizing the displacement by gravity forces. In 2006, Vicencio and Sepehmoori [22] investigated and simulated the injection of nitrogen in a fractured reservoir. Based on their results, the gravity drainage mechanism depended on nitrogen arrival time, depth of reservoir, and size of matrix block. Panfili and Cominelli [23] utilized an Embedded Discrete Fracture Model (EDFM) to simulate gas injection in a fractured reservoir. Based on their results, the proposed method of simulation, EDFM, was a cost-efficient and highly effective solution for the simulation of fracture reservoirs from an industrial viewpoint. Zhu et al. [24] proposed a novel gas injection scheme to improve oil recovery in shale. In this scheme, gas would be injected from one fracture, and oil will be produced from another fracture. Based on their results, the new proposed scheme resulted in improving oil recovery. Wan et al. [25] simulated the potential for enhanced oil recovery (EOR) in shale oil reservoirs through cyclic gas injection. Their results showed, as a contact volume of fracture with matrix was high, its contribution to good productivity was high. Mu et al. [26] introduced an analytical solution for the Buckley-Leverett (BL) equation in gas flooding, taking into consideration miscibility. Wide data analysis conducted by Ahdaya and Imqam [27] to determine the conditions that miscible injection could be applied. Based on their results, CO_2 was the most common injection gas in the miscible gas injection process. Their investigation showed the oil with API gravity of 35.1 to 45 ^{o}API and viscosity of 0.25 to 1.5 cP was used in the most experimental investigation. Mogensen and Xu [28] studied the miscible nitrogen flooding in a lower permeability, high-temperature carbonate reservoir. Based on their results, different behavior of nitrogen than other injection gas was revealed. They showed that MMP became constant when more than 35% of nitrogen is existed in a injection gas mixture. Kashkooli et al. [29] investigated capture and carbon storage-EOR and they used the dynamic well flow settings as the optimization variables. Based on their results, they proposed redefining the idea of "the more injection, the better". Their results showed the reduction of water production in the optimized case. They showed the fraction of CO_2 that both produced liquid and gas would be reduced in the optimized case.

Besides various methods have been developed to simulate the gas injection, BL is a simple analytical method. Based on some sensible and essential assumptions, the theory of fractional flow has been developed. The theory of fractional flow has been started with BL for water injection. Then this theory has been applied for different EOR methods like polymer flooding and gas flooding [30-35]. BL equation is known as an analytical solution for displacement front in two-phase flow. BL equation has been used widely to predict the advance of a fluid displacement front. The rate of penetration of injected water bank in porous media can be predicted by BL equation. In order to obtain an analytical solution for BL equation, some assumptions are considered: Two-phase flow is considered to be linear and horizontal, injection fluid is gas, both displacing and displaced fluid are immiscible, formation contains on a layer, the total flow rate is constant at all section of the medium, injected fluid, gas, is injected at the inlet of medium, porous media is considered to be incompressible, the effect of gravity and capillary pressure is negligible, there is no capillary transition zone and fingering, porous media has a finite length, and it is homogeneous, the boundary conditions of porous media are constant. [36]

Although there are several simulation studies in gas injection, the simple method that can consider both immiscible and miscible conditions and consider the impact of porous media is still missing. In this study, the BL method was employed to simulate the gas injection process under both miscible and immiscible conditions, and the impact of the porous media in the gas flooding process was examined. In order to consider the effect of miscibility, modification on the relative permeability and viscosity of fluid was implemented. In addition, IFT was modified to consider the impact of porous media.

In the present study, after conducting the validation, the impact of injection gas on the IFT was investigated. Afterward, the effect of IFT at MMP was investigated. The influence of porous media on the IFT and the effect of modified IFT was studied in the next section. Finally, conclusions of the present work were presented.

2. Mathematical model

In this section, a mathematical model and algorithm of study are presented. Fig. 1 shows the flow chart of the present study.

The mathematical model of this study is divided into three main sections: a) calculation of IFT, b) modification of relative permeability, c) calculation of fractional flow and saturation of gas.

Fig. 1: The flowchart of the numerical model

2.1 Calculation of IFT

IFT is known as one of the main parameters that affects the behavior of fluids in a reservoir. It has an essential role in the oil industry, specifically in EOR. Several methods, both experimental and mathematical methods, have been existed to calculate the IFT of hydrocarbon fluids. Two common methods for the calculation of IFT are rising bubble and pendant drop methods [37]. In the first method, a bubble will be upward in the denser phase. In the second one heavier phase must be suspended in the lighter phase, and then by using Young-Laplace equation, IFT can be determined [37]. In addition to different experimental methods for the calculation of IFT, several empirical correlations can estimate the IFT of system [37]. Ramey [38] modified Weinaug-Katz correlation for IFT, and in this study, Ramey's correlation was utilized to calculate the IFT of the oil-gas system:

$$\sigma_{go}^{\frac{1}{4}} = P_o\left(x_o \frac{\rho_o}{M_{og}} - y_o \frac{\rho_g}{M_{go}}\right) - P_g\left(x_g \frac{\rho_o}{M_{og}} - y_g \frac{\rho_g}{M_{go}}\right) \tag{1}$$

Where x_o, x_g, y_o, and y_g show mole fraction of components in the oil phase and gas phase, respectively. In the above equation, the density of oil and gas is showed by ρ_o and ρ_g, respectively. M_{og} and M_{go} denote the average molecular weight of oil and gas phase, respectively; P_o and P_g denote the Parachor equation suggested by Whitson and Brule; σ_{go} displays the IFT of oil and gas.

The following formula was used to calculate the aforementioned parameters [38, 39]:

$$M_o = \frac{6084}{(\gamma_{API} - 5.9)} \tag{2}$$

$$M_g = 28.97 \times \gamma_g \tag{3}$$

$$P_o = \left(2.376 + 0.0102 \times \gamma_{API}\right) \times M_o \tag{4}$$

$$P_g = \left(25.2 + 2.86 \times M_o\right) \tag{5}$$

$$x_o = \left(1 + \frac{7.521 \times 10^{-6} \times M_o \times R_s}{\gamma_o}\right)^{-1} \tag{6}$$

$$x_g = 1 - x_o \tag{7}$$

$$y_o = \left(1 + \frac{7.521 \times 10^{-6} \times M_o}{\gamma_o \times r_v}\right)^{-1} \tag{8}$$

$$y_g = 1 - y_o \tag{9}$$

$$\rho_o = \frac{\gamma_o + 2.179 \times 10^{-4} \times \gamma_g \times R_s}{B_o} \tag{10}$$

$$\rho_g = 9.3184 \times 10^{-2} \times \frac{P \times M_{go}}{62.4 \times Z \times T} \tag{11}$$

$$M_{og} = (x_o \times M_o + x_g \times M_g) \tag{12}$$

$$M_{go} = (y_o \times M_o + y_g \times M_g) \tag{13}$$

In the above equation, the molecular weight of gas and oil is shown by M_g and M_o, respectively. Here, R_s presents the solution gas-oil ratio, B_o represents oil formation volume factor, and γ_o denotes the specific gravity of the oil. The specific gravity of oil can be related to γ_{API}: $\gamma_{API} = \frac{141.5}{\gamma_o} - 131.5$. In addition, r_v represents vaporized oil in the gas phase. There is a general assumption is used with the black oil approach. In this assumption $r_v = 0$, therefore, $y_o = 1$, and $y_g = 0$. γ_g is the specific gravity of gas, and P, Z, and T display pressure, compressibility factor, and temperature. It is worthwhile to mention that there are several empirical correlations to compute the oil formation volume factor, compressibility factor, and solution gas-oil ratio. In our study, the following formula was used to calculate the above-mentioned parameters:

Sutton [40] suggested the following correlation to calculate critical temperature and pressure.

$$T_{pc} = 169.2 + 349.5 \times \gamma_g - 74 \times \gamma_g^2 \tag{14}$$

$$P_{pc} = 756.8 - 131.07 \times \gamma_g - 3.6 \times \gamma_g^2 \tag{15}$$

$$T_{pr} = \frac{T}{T_{pc}} \tag{16}$$

$$P_{pr} = \frac{P}{P_{pc}} \tag{17}$$

$$tpr = \frac{1}{T_{pr}} \tag{18}$$

In the above equation, T_{pc} and T_{pr} display pseudocritical and pseudoreduced temperature; P_{pc} and P_{pr} are pseudocritical and pesudoreduced pressure.

For the compressibility factor, Brill and Beggs' correlation was employed [41]:

$$Z = A + \frac{1-A}{e^B} + C \times P_{pr}^D \tag{19}$$

$$A = 1.39 \times \left(T_{pr} - 0.92\right)^{0.5} - 0.36 \times T_{pr} - 0.10 \tag{20}$$

$$B = \left(0.62 - 0.23 \times T_{pr}\right) \times P_{pr} + \left(\frac{0.066}{T_{pr} - 0.86} - 0.037\right) P_{pr}^2 + \frac{0.32 \times P_{pr}^2}{10^E} \tag{21}$$

$$C = 0.132 - 0.32 \times \log(T_{pr}) \tag{22}$$

$$D = 10^F \tag{23}$$

$$E = 9 \times \left(T_{pr} - 1\right) \tag{24}$$

$$F = 0.3106 - 0.49 \times T_{pr} + 0.1824 \times T_{pr}^2 \tag{25}$$

Brill and Beggs' correlation constants are represented by the letters A to F. The Standing correlation was utilized to compute the solution gas oil ratio and the formation volume factor [42]:

$$R_s = \gamma_g \times \left[\left(\frac{P}{18.2} + 1.4\right) \times 10^a\right]^{1.2048} \tag{26}$$

$$a = 0.00091 \times (T - 460) - 0.0125 \times \gamma_{API} \tag{27}$$

$$B_o = 0.9759 + 0.000120 \times \left[R_s \times \left(\frac{\gamma_g}{\gamma_o}\right)^{0.5} + 1.25 \times \left(T - 460\right)\right]^{1.2} \tag{28}$$

2.2 Calculation of the relative permeability of the gas-oil system

One of the main parameters affected by IFT is the relative permeability of the reservoir fluids. Researchers have been proposed different models to predict the relative permeability. Most of these models are tried to interpolate the relative permeability curves at the miscible and immiscible conditions. A first model in this type was proposed by Coats [43], and this model was a function of IFT:

$$K_{RO} = F_K \times K_{ro}^{imm} + (1 - F_K) \times K_{ro}^{mis} \tag{29}$$

$$K_{RG} = F_K \times K_{rg}^{imm} + (1 - F_K) \times K_{rg}^{mis} \tag{30}$$

Where K_{RO} is a modified oil relative permeability which considered a both miscible, K_{ro}^{mis}, and a immiscible, K_{ro}^{imm}, oil relative permeability. In addition, K_{RG} shows a modified gas relative permeability and the same as the modified oil relative permeability, both a miscible, K_{rg}^{mis}, and a immiscible, K_{rg}^{imm}, relative permeability are considered in these parameters. F_k is a relative permeability interpolation parameter that related to the IFT [43]:

$$F_K = \min\left[1, \left(\frac{\sigma}{\sigma_0}\right)^N\right] \tag{31}$$

In the above equation, σ and σ_0 are the IFT and the IFT at MMP, respectively [43].

$$S_{or} = F_K \times S_{or}^{imm} \tag{32}$$

$$S_{gi} = F_K \times S_{gi}^{imm} \tag{33}$$

$$S_{gn} = \frac{S_g - S_{gi}}{1 - S_{gi} - S_{or}} \tag{34}$$

Corey-Brooks [44] correlation was employed to compute the relative permeability of gas and oil under immiscible conditions:

$$K_{ro}^{imm} = K_{ro} \times \left(1 - S_{gn}\right)^{n_o} \tag{35}$$

$$K_{rg}^{imm} = K_{rg} \times S_{gn}^{n_g} \tag{36}$$

$$K_{ro}^{mis} = \left(1 - S_{gn}\right)^{n_m} \tag{37}$$

$$K_{rg}^{mis} = S_{gn}^{n_m} \tag{38}$$

S_{or} and S_{gi} are a modified residual oil saturation, and an iKrreducible gas-phase saturation, respectively, and S_{or}^{imm} and S_{gi}^{imm} display the same parameters at an immiscible conditions. K_{ro} and K_{rg} present an oil relative permeability at an irreducible gas saturation and a gas relative permeability at a residual oil saturation, respectively. n_g and n_o, are an gas and a oil exponent for the Brooks-Corey functions. These parameters can be obtained through an immiscible relative permeability curve. n_m is a releative permeability index and in this paper n_m is considered 1.1.

2.3 Calculating the viscosity of oil and gas

The injection of gas results in a decrease in the viscosity of the oil, making it crucial to modify the viscosity of both the oil and gas for accurately simulating the gas injection process. In the present study, Todd-Longstaff [45] model was employed to calculate the effective gas and oil viscosity:

$$\mu_{oeff} = \mu_o^{1-\omega} \times \mu_m^{\omega} \tag{39}$$

$$\mu_{geff} = \mu_g^{1-\omega} \times \mu_m^{\omega} \tag{40}$$

$$\left(\frac{1}{\mu_m}\right)^{\frac{1}{4}} = \frac{S_g^{'}}{S_n^{'}} \times \left(\frac{1}{\mu_g}\right)^{\frac{1}{4}} + \frac{S_o^{'}}{S_n^{'}} \times \left(\frac{1}{\mu_o}\right)^{\frac{1}{4}} \tag{41}$$

$$S_o^{'} = S_o - S_{or} \tag{42}$$

$$S_g^{'} = S_g - S_{gi} \tag{43}$$

$$S_n^{'} = S_o^{'} - S_g^{'} \tag{44}$$

Here μ_m shows a mixing viscosity and ω presents a mixing factor of the viscosity, and in this study, $\omega = \frac{1}{3}$. In addition, the fluids effective viscosity and the fluids viscosity are presented by μ_{oeff}, μ_{oeff}, μ_{oeff}, and μ_{oeff}, respectively.

2.4 Calculating saturation and fractional flow of gas

The BL equation was employed to measure the fractional flow of gas and gas saturation. Derivation of the equation can be found in the different literature. The final formulas that were used in this study are as follows [36]:

$$f_g = \frac{S_g^2}{S_g^2 + (1+S_g)^2 \times V} \tag{45}$$

$$\frac{df_g}{dS_g} = \frac{2 \times V \times \left(S_g - 1\right) \times S_g}{\left(V \times \left(S_g - 1\right)^2 + S_g^2\right)^2} \tag{46}$$

$$PVI = \frac{q_t \times t}{Area \times L \times \phi} \tag{47}$$

$$x_{sg} = PVI \times L \times \left(\frac{df_g}{dS_g}\right)_{S_g} \tag{48}$$

In the above equation, f_g shows a fractional flow of gas; $\frac{df_g}{dS_g}$ denotes the derivative of the fractional flow of gas with respect to the gas saturation; V is a ratio of the viscosity $(\frac{\mu_g^{eff}}{\mu_o^{eff}})$; PVI is a dimensionless pore volume injection, $Area$, L, and ϕ display a cross-section area, length of the domain, and porosity of the domain, respectively; q_t and t show a total injection rate and an injection time. In addition, x_{Sg} shows a distance moved by a specific S_g contour.

3. Results and discussion

3.1 Numerical simulation

Each step of the numerical simulation is shown in Fig. 1, and the inputs parameters are presented in Table 1.

Table 1: Input parameters and their values used in numerical simulation

Model validation is the first step in an each simulation study. Hence, some of the existing experimental findings and simulation studies were utilized to validate the developed model. The first step involved evaluating the developed model for the density of reservoir oil, oil formation volume factor, and solution gas-oil ratio using existing experimental data. Fig. 2 shows the comparison between the experimental value of the density of oil, oil formation volume factor, solution gas-oil ratio, and fluid's relative permeability with their predicted value. As shown in Fig. 2, the developed model in this study can predict the above-mentioned properties very well, and its error in the prediction is low.

Fig. 2: a) Experimental and predicted oil density vs. pressure, experimental and predicted oil formation volume factor vs. pressure, solution gas-oil ratio vs. pressure,, and relative permeability of oil and gas versus saturation

In the last step of validation, the predicted fractional flow curve of the present study compare with the result of Mu et al. [26]. Fig. 3 shows the comparison of the fractional flow, and a good match between Mu et al.'s study and our study is seen.

Fig. 3: Comparison predicted fractional flow of present study with Mu et al. [26]

3.2 Effect of injection gas on the IFT

This section presents an investigation into the impact of injection gas on IFT and, consequently, on the relative permeability of gas and oil, gas saturation profile, and gas fractional flow. Fig. 4 shows the IFT between different injection gases and oil.

Fig. 4: IFT between oil and injected gases

As shown in Fig. 4, MMP of carbon dioxide is less than two other gases, and methane has higher MMP than nitrogen. Based on Fig. 4, near miscible pressure and IFT at MMP (IFT0) of three-injection gas were determined. We determined the near miscible pressure based on the point that the IFT reached the value of less than 1 mN/m. Therefore, for carbon dioxide, nitrogen, and methane, IFT0 was 0.99 at a pressure of 796, 1518, and 3351 psi, respectively. In order to study the impact of injection gases on the relative permeability, saturation curve and fractional flow of gas, three injection pressures, 500, 1000 and 5000 psi, were used. At 500 psi, F_k was 1 (based the Equation (31)); therefore, the immiscible situation was dominated. As shown in Fig. 5, once injected gases were in the immiscible condition, there was not seen any impact on fractional flow, saturation, and relative permeability curves.

Fig. 5: Impact of injection gas on fractional flow, saturation, and relative permeability curves at injection pressure of 500 psi

The second scenario involved injecting gas at a pressure of 1000 psi. Based on the Equation (31), in this situation, CO_2 is injected as the miscible gas, while N_2 and CH_4 are injected as the immiscible gases. As shown in Fig. 6, CO_2 resulted in an alteration in the relative permeability of oil and gas and shifted their relative permeability to the right side. Additionally, when CO_2 was used as an injected gas, a breakthrough occurred (subplot (b) of Fig. 6). Furthermore, the effect of CO_2 in miscible conditions on the fractional flow curve is shown in subplot (c) of Fig. 6. CO_2 is heavier than two other gases, therefore sooner than two other ones reach to the miscible condition. As it is injected in the miscible conditions, it moves faster in a porous media. Therefore, at the same time, it reaches the end of the domain and has a breakthrough. In addition, it increases the relative permeability of oil more than the other two gases.

Fig. 6: Impact of injection gas on fractional flow, saturation, and relative permeability curves at injection pressure of 1000 psi

The injection pressure in the last scenario was set at 5000 psi, as depicted in Fig. 7. In this scenario, all gasses are injected in the miscible conditions. As shown in subplot (a) of Fig. 7, oil relative permeability once injection gas was CO2, lied on the left side of other gases' oil relative permeability. In addition, gas relative permeability in a scenario that CO2 was used as an injection gas was staying out on the right side of other gases. Oil and gas relative permeability for a scenario in which CH_4 was the injection fluid was between two other gases' relative permeability. The impact of injection fluid on the fractional flow curve is presented in subplot (c) of Fig. 7. By increasing the injection pressure, all three gases are injected as the miscible gases, a breakthrough of all gases occurred (Subplot (b) of Fig. 7). In this case, the relative permeability of gas shifted to the left, while the relative permeability of oil shifted to the right due to the presence of nitrogen and methane. The impact of nitrogen on fractional flow, saturation, and relative permeability curves is more than two other gases. Carbon dioxide, as the heavier gas among three injection gases, has less impact on fractional flow, saturation, and relative permeability curves. The primary reason for this phenomenon is that carbon dioxide has a lower IFT than the other two gases.

Fig. 7: Impact of injection gas on fractional flow, saturation, and relative permeability curves at injection pressure of 5000 psi

3.3 Effect of IFT0

Four IFT0 for three gases were studied to investigate the effect of the IFT at MMP on fractional flow, saturation, and relative permeability curves. Fig. 8-Fig. 11 show the impact of IFT0 on fractional flow, saturation, and relative permeability curves. The injection pressures were 500, 1000, 3000, and 5000 psi and carbon dioxide was used as an injection fluid. As shown in subplot (a) of Fig. 8 through Fig. 11, an increase in the IFT0 results in decrease in the relative permeability of oil and an increase in the relative permeability of gas. There is no clear difference between IFT0 of 0.001 and 1 in this case. The front of gas at higher IFT0 was more than the lower one. Therefore, higher IFT0 resulted in more distance move by the injection gas at the same conditions (Subplot (b) of Fig. 8-Fig. 11). Subplot (c) of Fig. 8-Fig. 11 show increasing in the IFT0 shifted the fractional flow curve.

Fig. 8: Impact of IFT0 on fractional flow, saturation, and relative permeability curves for carbon dioxide at an injection pressure of 500 psi

Fig. 9: Impact of IFT0 on fractional flow, saturation, and relative permeability curves for carbon dioxide at an injection pressure of 1000 psi

Fig. 10: Impact of IFT0 on fractional flow, saturation, and relative permeability curves for carbon dioxide at an injection pressure of 3000 psi

Fig. 11: Impact of IFT0 on fractional flow, saturation, and relative permeability curves for carbon dioxide at an injection pressure of 5000 psi

The same as Fig. 8-Fig. 11, Fig. 12-Fig. 15 show the impact of IFT0 at different injection pressures on fractional flow, saturation, and relative permeability curves. In this part, methane was used as an injection fluid. As shown in Fig. 12 and Fig. 13, IFT0 is not affected in the outputs of the model. However, by increasing the injection pressure, 3000 and 5000 psi, the effect of IFT0 on each curve is evident. In other words, by increasing the injection pressure, the injection gas moves to miscible conditions; therefore, its effect on the outputs of the model was observed. Hence, if gas is injected in the immiscible conditions, the effect of IFT0 on the outputs of the model is negligible. Nevertheless, if the injection pressure is increased and the gas transitions to the miscible condition, the impact of IFT0 becomes apparent.

Fig. 12: Impact of IFT0 on fractional flow, saturation, and relative permeability curves for methane at an injection pressure of 500 psi

Fig. 13: Impact of IFT0 on fractional flow, saturation, and relative permeability curves for methane at an injection pressure of 1000 psi

Fig. 14: Impact of IFT0 on fractional flow, saturation, and relative permeability curves for methane at an injection pressure of 3000 psi

Fig. 15: Impact of IFT0 on fractional flow, saturation, and relative permeability curves for methane at an injection pressure of 5000 psi

The impact of IFT0 on fractional flow, saturation, and relative permeability curves at the different pressures and once N_2 was used as an injection fluid is presented in Fig. 16-Fig. 19. At first injection pressure, 500 psi, the effect of IFT0 is negligible. By increasing the injection pressure, alteration on fractional flow, saturation, and relative permeability curves is obvious. Similar to the other two gases, increasing the injection pressure for nitrogen and transitioning to the miscible condition impacts the fractional flow, saturation, and relative permeability curves.

Fig. 16: Impact of IFT0 on fractional flow, saturation, and relative permeability curves for nitrogen at an injection pressure of 500 psi

Fig. 17: Impact of IFT0 on fractional flow, saturation, and relative permeability curves for nitrogen at an injection pressure of 1000 psi

Fig. 18: Impact of IFT0 on fractional flow, saturation, and relative permeability curves for nitrogen at an injection pressure of 3000 psi

Fig. 19: Impact of IFT0 on fractional flow, saturation, and relative permeability curves for nitrogen at an injection pressure of 5000 psi

3.4 Effect of modified IFT

In the most experimental and simulation studies, IFT of the bulk medium was used for calculation, and the effect of porous media was missed. However, the property of the porous media, i.e., porosity and permeability, affected the IFT. This section presents the modification of IFT for CO2 injection, taking into account the effect of porous media, using the developed code. Afterward, based on modified IFT, fractional flow, saturation, and relative permeability curves were recalculated. As the developed code calculated the IFT of bulk and porous media-based compositional model, we used compositional model for the bulk medium. Therefore, we can have a better comparison between IFT of the bulk and the porous media. r_p was used to show the impact of the porous media on the IFT:

$$r_p = \sqrt{\frac{k}{\phi}} \tag{49}$$

Where k and φ show permeability and porosity, respectively. Based on Table 1, for our porous media, the value of r_p is 10. Table 2 shows the IFT of crude oil- CO_2 at two different pressure for the both bulk and the porous media.

Table 2: IFT of crude oil-CO_2 at two-injection pressure for bulk and porous media

Fig. 20 and Fig. 21 show the impact of the bulk and the porous media on fractional flow, saturation, and relative permeability curves at two injection pressures of 500 and 1000 psi. It is worthwhile to mention that in the both cases, the value of the IFT0 was 1.

Fig. 20: Impact of bulk and porous media on fractional flow, saturation, and relative permeability curves for carbon dioxide as an injection gas at an injection pressure of 500 psi

Fig. 21: Impact of bulk and porous media on fractional flow, saturation, and relative permeability curves for carbon dioxide as an injection gas at an injection pressure of 1000 psi

As shown in Table 2, the medium has an effect on IFT; however, the influence of medium on fractional flow, saturation, and relative permeability curves was negligible. The primary reason for this phenomenon is F_K, which influences fractional flow, saturation, and relative permeability curves. As the value of F_K or both mediums was the same, no significant effect on the aforementioned curves was observed.

3.5 Effect of fracture

This section presents an investigation into the impact of fractures on IFT, fractional flow, saturation, and relative permeability curves. In this study, k and φ for the fracture reservoir are 13.57 md and 0.1638; therefore, the r_p of the fracture medium is 3000. Table 3 shows the IFT of crude oil-CO_2 for the fracture medium in two-injection rate.

Table 3: IFT of crude oil-CO_2 at two-injection pressure for fracture media

Fig. 22 presents the effect of the fracture on fractional flow, saturation, and relative permeability curves. As shown in Table 3, in both injection pressure, the IFT is more than IFT0; therefore, there is not seen any effect of two different injection pressures on the aforementioned curves.

Fig. 22: Impact of fracture medium on fractional flow, saturation, and relative permeability curves for carbon dioxide as an injection gas at an injection pressure of 500 psi and 1000 psi

In the present study, based on BL method, a process of gas injection in the both miscible and the immiscible conditions was studied. Modification on the relative permeability and viscosity of fluids cause the developed code can investigate the gas injection in the immiscible, miscible, and the near miscible conditions. This advantage of the developed code can give a suitable view of the performance of the injection gas before the process of EOR in the reservoir. By this modification, the performance of each injection gas at the various conditions can be checked and bases on the achieved results a suitable decision can be get for the selection of EOR method. Another advantage of the developed code is considering the impact of porous media. By considering the effect of the porous media on gas injection process, accurate simulation of gas injection in the reservoir can be achieved. In order to better simulate and mimic the process of the gas injection, variations in the composition of injection and reservoir fluids during gas injection must be considered and investigated. In the developed code, the mechanism of gas injection cannot be investigated and determined.

4. Conclusions

The current study investigated the gas flooding process, focusing on the effects of different gases, modified IFT, and IFT at MMP, on fractional flow, saturation, and relative permeability curves. The key findings of this study can be summarized as follows:

1. Different gases resulted in different IFT and MMP. Methane has higher IFT and lower IFT belongs to carbon dioxide. The primary reason for this phenomenon is the molecular weight of the gases. Carbon dioxide has a higher molecular weight and lower IFT than the other two gases. However, methane has a lower molecular weight, and it has higher IFT.

2. Under an injection pressure of 500 psi, the injection gas had no discernible impact on the fractional flow, saturation, and relative permeability curves. However, increasing the injection pressure to 1000 psi resulted in fractional flow, saturation, and relative permeability curves being influenced by the injection gas.

3. Nitrogen and methane have lower molecular weight than carbon dioxide, therefore shift relative permeability of gas to the right side and the relative permeability of oil to the left side.

4. Carbon dioxide as a heavier gas resulted to breakthrough at injection pressure of 1000 psi.

5. The impact of injection gas on fractional flow, saturation, and relative permeability curves is dependent on factors such as injection pressure, IFT0, and the condition of the injection gas. At injection pressure of 500 psi, all three gases are in immiscible condition. IFT0, IFT at near miscible pressure, is lower than the IFT of each gas and F_k was 1; therefore, there was not any difference among injection gases. However, by increasing injection pressure, fractional flow, saturation, and relative permeability curves affected by injection gases. In other words, IFT0 can affected the output of model in the miscible conditions.

6. Porous media and fracture affected IFT severely, however as IFT0 was 1, F_k for both medium and injection pressure was the same. Therefore, the impact of these mediums on fractional flow, saturation, and relative permeability curves is negligible.

Acknowledgements

The authors would like to extend their gratitude to Iran's National Elites Foundation for providing financial support for this study.

Abbreviations

Nomenclature

EOR = Enhanced Oil Recovery

MMP = Minimum miscibility pressure

MME = Minimum miscibility enrichment

BL = Buckley-Leverett

Symbols

x_o = Mole fraction of oil in oil phase

x_g = Mole fraction of gas in oil phase

y_o = Mole fraction of oil in gas phase

y_g = Mole fraction of gas in gas phase

ρ_o = Density of oil phase, $\frac{lbm}{ft^3}$

ρ_g = Density of gas phase, $\frac{lbm}{ft^3}$

M_{og} = Average molecular weight of oil phase, $\frac{lbm}{lbmol}$

M_{go} = Average molecular weight of gas phase, $\frac{lbm}{lbmol}$

P_o = Parachor equation for oil phase

P_g = Parachor equation for gas phase

σ_{go} = IFT of gas and oil, $\frac{dynes}{cm}$

M_o = Molecular weight of oil phase, $\frac{lbm}{lbmol}$

M_g = Molecular weight of gas phase, $\frac{lbm}{lbmol}$

R_s = Solution gas oil ratio, $\frac{scf}{STB}$

B_o = Oil formation volume factor, $\frac{bbl}{STB}$

γ_o = Specific gravity of oil

γ_g = Specific gravity of gas

γ_{API} = American Petroleum Institute

r_v = Vaporized oil in the gas phase, $\frac{scf}{STB}$

p = Pressure, $psia$

Z = Compressibility factor

T = Temperature, R

P = Pressure, $psia$

T_{pc} = Pseudocritical temperature, R

P_{pc} = Pseudocritical pressure, $psia$

T_{pr} = Pseudoreduced temperature

P_{pr} = Pseudoreduced pressure

A-F = Constants for Brill and Beggs' calculation to calculate compressibility factors

K_{RO} = Oil relative permeability

K_{RG} = Gas relative permeability

K_{ro}^{mis}= Miscible oil relative permeability

K_{rg}^{mis}= Miscible gas relative permeability

K_{ro}^{imm}= Immiscible oil relative permeability

K_{rg}^{imm}= Immiscible gas relative permeability

F_k = Relative permeability interpolation parameter

σ_0 = Interfacial tension at minimum miscible pressure, $\frac{dynes}{cm}$

σ = Interfacial tension at different pressure, $\frac{dynes}{cm}$

S_{or} = Residual oil saturation

S_{gi} = Irreducible gas phase saturation

S_{or}^{imm}= Residual oil saturation at immiscible condition

S_{gi}^{imm}= Irreducible gas phase saturation at immiscible condition

K_{ro} = Oil relative permeability at irreducible gas saturation

K_{rg} = Gas relative permeability at residual oil saturation

n_o = Gas exponent for Brooks-Corey functions

n_g = Oil exponent for Brooks-Corey functions

n_m = Relative permeability index

n_m = Read-in exponent

μ_{oeff} = Oil effective viscosity, $mPa.s$

μ_{geff} = Oil effective viscosity, $mPa.s$

μ_o = Oil viscosity, $mPa.s$

μ_g = Gas viscosity, $mPa.s$

μ_m = Mixing viscosity, $mPa.s$

ω = Mixing factor

f_g = Fractional flow of gas

$\frac{df_g}{dS_g}$ = Derivative of the fractional flow of gas with respect to gas saturation

V = Viscosity ratio

PVI = Dimensionless pore volume

$Area$ = Cross section area, m^2

L = Length of investigated domain, m

ϕ = Porosity of domain, %

q_t = Total injection rate, $\frac{m^3}{hr}$

t = Injection time, hr

x_{S_g} = Distance moved by a specific S_g contour, m

Reference

1. Kamali, F., Cinar, Y., "Co-optimizing enhanced oil recovery and CO2 storage by simultaneous water and CO2 injection", *Energy exploration & exploitation*, **32** (2), pp. 281-300, (2014).

2. Zhao, X., Rui, Z., Liao, X., "Case studies on the CO2 storage and EOR in heterogeneous, highly water-saturated, and extra-low permeability Chinese reservoirs", *Journal of Natural Gas Science and Engineering*, **29**, pp. 275-283, (2016).
3. Holm, L., "Miscibility and miscible displacement", *Journal of Petroleum Technology*, **38** (08), pp. 817-818, (1986).
4. Green, D. W., Willhite, G. P., "Enhanced oil recovery", Henry L. Doherty Memorial Fund of AIME, Society of Petroleum Engineers, pp. (1998)
5. Klins, M. A., "Carbon dioxide flooding: Basic mechanisms and project design", pp. (1984).
6. Sheng, J. J., "Enhanced oil recovery field case studies", Gulf Professional Publishing, pp. (2013)
7. Safaei, A., Kazemzadeh, Y., Riazi, M., "Mini Review of Miscible Condition Evaluation and Experimental Methods of Gas Miscible Injection in Conventional and Fractured Reservoirs", *Energy & Fuels*, **35** (9), pp. 7340-7363, (2021).
8. Shariatpanahi, S. F., Dastyari, A., Bashukooh, B., et al., *Visualization experiments on immiscible gas and water injection by using 2D-fractured glass micromodels*, in *SPE Middle east oil and gas show and conference*, (2005).
9. Dastyari, A., Bashukooh, B., Shariatpanahi, S. F., et al., *Visualization of gravity drainage in a fractured system during gas injection using glass micromodel*, in *SPE Middle East Oil and Gas Show and Conference* (2005).
10. Nematzadeh, M., Khanamiri, H., Aghajani, M., et al., "An experimental study of secondary WAG injection in a low-temperature carbonate reservoir in different miscibility conditions", *Petroleum science and technology*, **30** (13), pp. 1359-1368, (2012).
11. Motealleh, M., Kharrat, R., Gandomkar, A., et al., "An experimental study on the applicability of water-alternating-CO2 injection in the secondary and tertiary recovery in one Iranian reservoir", *Petroleum science and technology*, **30** (24), pp. 2571-2581, (2012).
12. Yu, Y., Li, L., Sheng, J. J., "A comparative experimental study of gas injection in shale plugs by flooding and huff-n-puff processes", *Journal of Natural Gas Science and Engineering*, **38**, pp. 195-202, (2017).
13. Fahandezhsaadi, M., Amooie, M. A., Hemmati-Sarapardeh, A., et al., "Laboratory evaluation of nitrogen injection for enhanced oil recovery: Effects of pressure and induced fractures", *Fuel*, **253**, pp. 607-614, (2019).
14. Wang, L., He, Y., Wang, Q., et al., "Multiphase flow characteristics and EOR mechanism of immiscible CO2 water-alternating-gas injection after continuous CO2 injection: A micro-scale visual investigation", *Fuel*, **282**, pp. 118689, (2020).
15. Li, D., Saraji, S., Jiao, Z., et al., "CO2 injection strategies for enhanced oil recovery and geological sequestration in a tight reservoir: An experimental study", *Fuel*, **284**, pp. 119013, (2021).
16. Mahzari, P., Mitchell, T. M., Jones, A. P., et al., "Novel laboratory investigation of huff-n-puff gas injection for shale oils under realistic reservoir conditions", *Fuel*, **284**, pp. 118950, (2021).
17. Gandomkar, A., Sharif, M., "Nano composites performance as direct thickeners for gas based enhanced oil recovery, a new approach", *Journal of Petroleum Science and Engineering*, **194**, pp. 107491, (2020).
18. Chen, X., Mohanty, K. K., "Pore-scale mechanisms of immiscible and miscible gas injection in fractured carbonates", *Fuel*, **275**, pp. 117909, (2020).
19. Zhao, Y., Fan, G., Song, K., et al., "The experimental research for reducing the minimum miscibility pressure of carbon dioxide miscible flooding", *Renewable and Sustainable Energy Reviews*, **145**, pp. 111091, (2021).
20. Uleberg, K., Høier, L., *Miscible gas injection in fractured reservoirs*, in *SPE/DOE Improved Oil Recovery Symposium*, (2002).

21. Vicencio, O., Sepehrnoori, K., Miller, M., *Simulation of nitrogen injection into naturally fractured reservoirs*, in *SPE International Petroleum Conference in Mexico*, (2004).
22. Vicencio, O. A., Sepehrnoori, K., *Simulation of nitrogen injection into naturally fractured reservoirs based on uncertain properties and proper matrix grid resolution*, in *International Oil Conference and Exhibition in Mexico*, (2006).
23. Panfili, P., Cominelli, A., *Simulation of miscible gas injection in a fractured carbonate reservoir using an embedded discrete fracture model*, in *Abu Dhabi International Petroleum Exhibition and Conference*, (2014).
24. Zhu, P., Balhoff, M. T., Mohanty, K. K., "Compositional modeling of fracture-to-fracture miscible gas injection in an oil-rich shale", *Journal of Petroleum Science and Engineering*, **152**, pp. 628-638, (2017).
25. Wan, T., Sheng, J. J., Soliman, M., *Evaluate EOR potential in fractured shale oil reservoirs by cyclic gas injection*, in *Unconventional Resources Technology Conference*, pp. 1845-1854, (2013).
26. Mu, L., Liao, X., Chen, Z., et al., "Analytical solution of Buckley-Leverett equation for gas flooding including the effect of miscibility with constant-pressure boundary", *Energy exploration & exploitation*, **37** (3), pp. 960-991, (2019).
27. Ahdaya, M., Imqam, A., *Miscible gas injection application for enhanced oil recovery: Data analysis*, in *54th US Rock Mechanics/Geomechanics Symposium*, (2020).
28. Mogensen, K., Xu, S., "Comparison of three miscible injectants for a high-temperature, volatile oil reservoir-With particular emphasis on nitrogen injection", *Journal of Petroleum Science and Engineering*, **195**, pp. 107616, (2020).
29. Kashkooli, S. B., Gandomkar, A., Riazi, M., et al., "Coupled optimization of carbon dioxide sequestration and CO2 enhanced oil recovery", *Journal of Petroleum Science and Engineering*, **208**, pp. 109257, (2022).
30. Buckley, S. E., Leverett, M., "Mechanism of fluid displacement in sands", *Transactions of the AIME*, **146** (01), pp. 107-116, (1942).
31. Ehlig-Economides, C., Economides, M. J., "Sequestering carbon dioxide in a closed underground volume", *Journal of Petroleum Science and Engineering*, **70** (1-2), pp. 123-130, (2010).
32. Ghanbarnezhad, R., Lake, L. W., "Applying fractional-flow theory under the loss of miscibility", *Spe Journal*, **17** (03), pp. 661-670, (2012).
33. Hirasaki, G. J., "Application of the theory of multicomponent, multiphase displacement to three-component, two-phase surfactant flooding", *Society of Petroleum Engineers Journal*, **21** (02), pp. 191-204, (1981).
34. Johansen, T. E., James, L. A., Liu, X., "On the Buckley-Leverett equation with constant-pressure boundary conditions", *Spe Journal*, **21** (06), pp. 2301-2307, (2016).
35. Pope, G. A., "The application of fractional flow theory to enhanced oil recovery", *Society of Petroleum Engineers Journal*, **20** (03), pp. 191-205, (1980).
36. Dandekar, A. Y., "Petroleum reservoir rock and fluid properties", CRC press, (2013)
37. Drelich, J., Fang, C., White, C., "Measurement of interfacial tension in fluid-fluid systems", *Encyclopedia of surface and colloid science*, **3**, pp. 3158-3163, (2002).
38. Ramey Jr, H., "Correlations of surface and interfacial tensions of reservoir fluids", *Society of Petroleum Engineers*, (1973).
39. Whitson, C. H., Brulé, M. R., "Phase behavior", Henry L. Doherty Memorial Fund of AIME, Society of Petroleum Engineer, (2000)
40. Sutton, R., *Compressibility factors for high-molecular-weight reservoir gases*, in *SPE Annual Technical Conference and Exhibition*, (1985).
41. Beggs, D. H., Brill, J. P., "A study of two-phase flow in inclined pipes", *Journal of Petroleum Technology*, **25** (05), pp. 607-617, (1973).

42. Standing, M., *A pressure-volume-temperature correlation for mixtures of California oils and gases*, in *Drilling and Production Practice*, (1947).
43. Coats, K. H., "An equation of state compositional model", *Society of Petroleum Engineers Journal*, **20** (05), pp. 363-376, (1980).
44. Brooks, R. H., "Hydraulic properties of porous media", Colorado State University, pp. (1965)
45. Todd, M., Longstaff, W., "The development, testing, and application of a numerical simulator for predicting miscible flood performance", *Journal of Petroleum Technology*, **24** (07), pp. 874-882, (1972).

Tables and figures caption

Tables:

Table 1: Inputs parameters and their values used in numerical simulation

Table 2: IFT of crude oil-CO2 at two-injection pressure for bulk and porous media

Table 3: IFT of crude oil-CO2 at two-injection pressure for fracture media

Figures:

Fig. 1: The flowchart of the numerical model

Fig. 2: a) Experimental and predicted solution gas-oil ratio vs. pressure, b) Experimental and predicted oil formation volume factor vs. pressure, c) experimental and predicted oil density vs. pressure

Fig. 3: Schematic of an ANFIS model with two inputs parameter three injection pressures of 14, 22, and 30 MPa

Fig. 4: IFT between oil and injected gases

Fig. 5: Effect of injection gas on fractional flow, saturation, and relative permeability curves at injection

pressure of 500 psi

Fig. 6: Effect of injection gas on fractional flow, saturation, and relative permeability curves at injection pressure of 1000 psi

Fig. 7: Effect of injection gas on fractional flow, saturation, and relative permeability curves at injection pressure of 5000 psi

Fig. 8: Effect of IFT0 on fractional flow, saturation, and relative permeability curves for carbon dioxide at an injection pressure of 500 psi

Fig. 9: Effect of IFT0 on fractional flow, saturation, and relative permeability curves for carbon dioxide at an injection pressure of 1000 psi

Fig. 10: Effect of IFT0 on fractional flow, saturation, and relative permeability curves for carbon dioxide at an injection pressure of 3000 psi

Fig. 11: Effect of IFT0 on fractional flow, saturation, and relative permeability curves for carbon at an injection pressure of 5000 psi

Fig. 12: Effect of IFT0 on fractional flow, saturation, and relative permeability curves for methane at an injection pressure of 500 psi

Fig. 13: Effect of IFT0 on fractional flow, saturation, and relative permeability curves for methane at an injection pressure of 1000 psi

Fig. 14: Effect of IFT0 on fractional flow, saturation, and relative permeability curves for methane at an injection pressure of 3000 psi

Fig. 15: Effect of IFT0 on fractional flow, saturation, and relative permeability curves for methane at an injection pressure of 5000 psi

Fig. 16: Effect of IFT0 on fractional flow, saturation, and relative permeability curves for nitrogen at an injection pressure of 500 psi

Fig. 17: Effect of IFT0 on fractional flow, saturation, and relative permeability curves for nitrogen at an injection pressure of 1000 psi

Fig. 18: Effect of IFT0 on fractional flow, saturation, and relative permeability curves for nitrogen at an injection pressure of 3000 psi

Fig. 19: Effect of IFT0 on fractional flow, saturation, and relative permeability curves for nitrogen at an injection pressure of 5000 psi

Fig. 20: Effect of bulk and porous media on fractional flow, saturation, and relative permeability curves for carbon dioxide as an injection gas at an injection pressure of 500 psi

Fig. 21: Effect of bulk and porous media on fractional flow, saturation, and relative permeability curves for carbon dioxide as an injection gas at an injection pressure of 1000 psi

Fig. 22: Effect of fracture medium on fractional flow, saturation, and relative permeability curves for carbon dioxide as an injection gas at an injection pressure of 500 psi and 1000 psi

Table 1

Inputs parameters	**Value**
$\boldsymbol{P_b}$ (Bubble point pressure)	1379 psi
$\boldsymbol{T_{res}}$ (Reservoir temperature)	643.77 R
$\boldsymbol{API}$ (API of reservoir oil)	19.96
$\boldsymbol{L}$ (Length of the simulated domain)	200 m
$\boldsymbol{\mu_o}$ (Oil viscosity)	1.81 mPa.s
$\boldsymbol{\mu_g}$ (Gas viscosity)	0.035 mPa.s
$\boldsymbol{K_{ro}}$ (Oil relative permeability at irreducible gas saturation)	0.9
$\boldsymbol{K_{rg}}$ (Gas relative permeability at residual oil saturation)	0.6181
$\boldsymbol{S_{or}}$ (Residual oil saturation)	0.24
$\boldsymbol{S_{oi}}$ (Initial saturation of oil)	0.95
$\boldsymbol{S_{gi}}$ (Initial saturation of gas)	0.05
$\boldsymbol{n_o}$	2.1079
$\boldsymbol{n_g}$	2.9852
N	1/4
$\boldsymbol{k}$	20 md
$\boldsymbol{\varphi}$	0.2

Table 2

Injection pressure (psi)	IFT of bulk media (mN/m)	IFT of porous media (mN/m)
500	9.48	3.13
1000	7.26	2.18

Table 3

Injection pressure (psi)	**IFT of fracture media (mN/m)**
500	9.38
1000	7.18

746
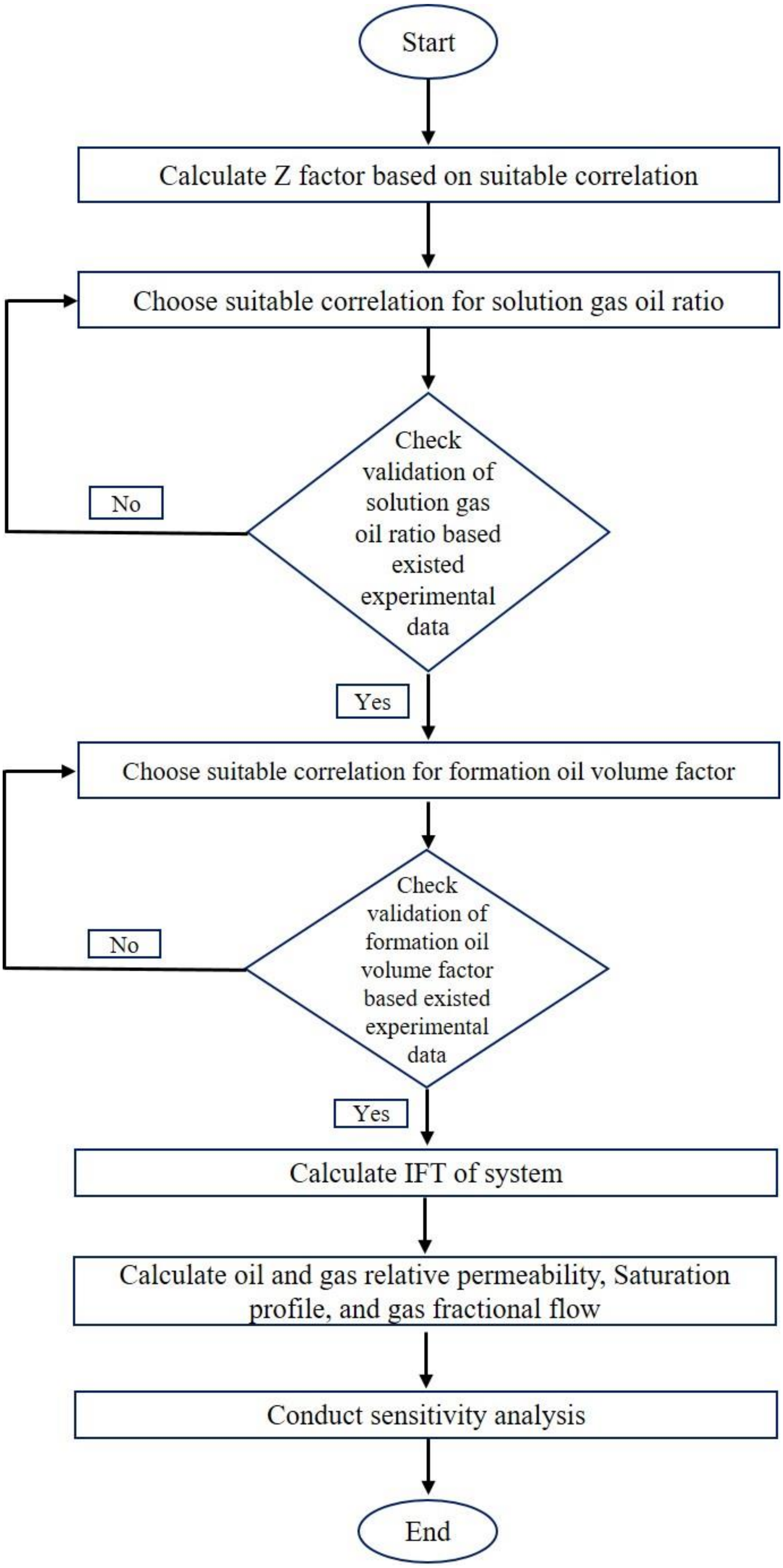
Start
Calculate Z factor based on suitable correlation
Choose suitable correlation for solution gas oil ratio
Check validation of solution gas oil ratio based existed experimental data
No
Yes
Choose suitable correlation for formation oil volume factor
Check validation of formation oil volume factor based existed experimental data
No
Yes
Calculate IFT of system
Calculate oil and gas relative permeability, Saturation profile, and gas fractional flow
Conduct sensitivity analysis
End

747 Fig.1

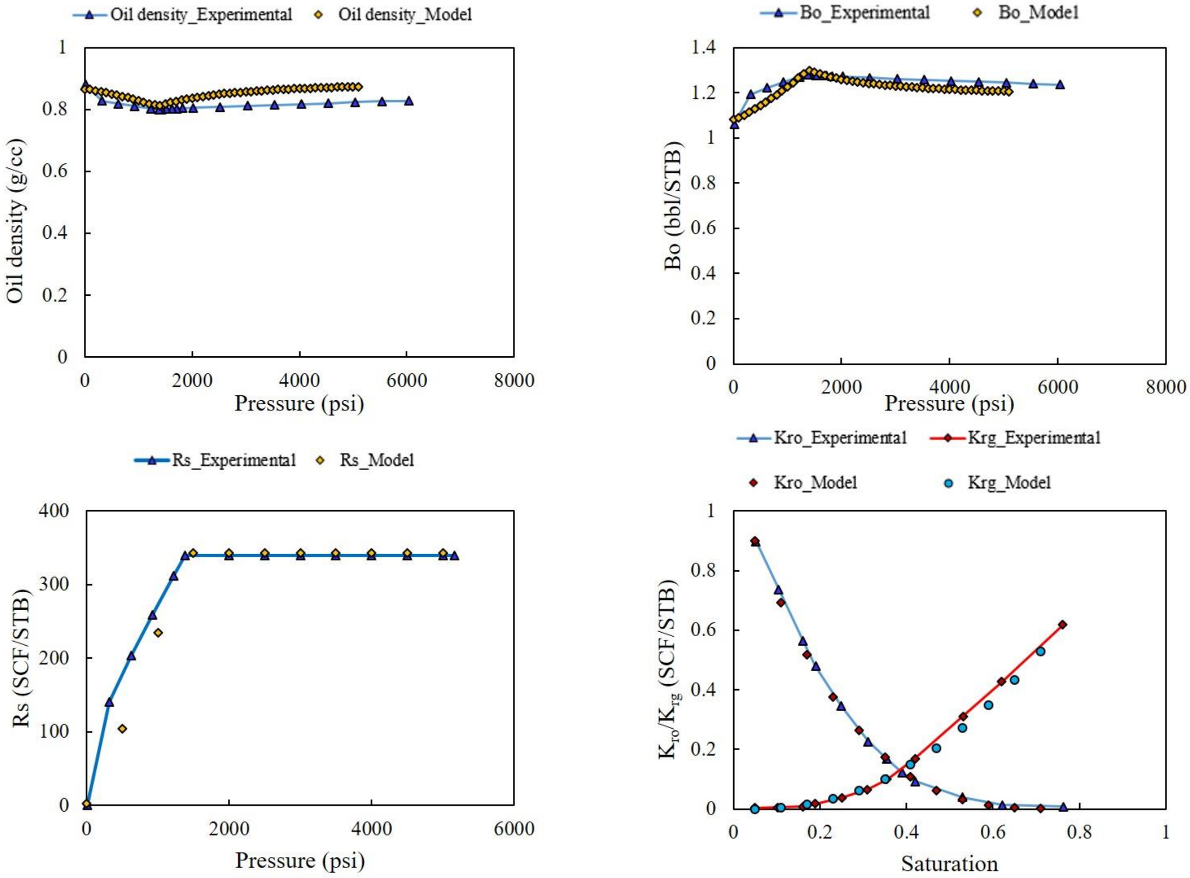
Oil density_Experimental
Oil density_Model
Oil density (g/cc)
Pressure (psi)
Bo_Experimental
Bo_Model
Bo (bbl/STB)
Pressure (psi)
Rs_Experimental
Rs_Model
Rs (SCF/STB)
Pressure (psi)
Kro_Experimental
Krg_Experimental
Kro_Model
Krg_Model
K_{ro}/K_{rg} (SCF/STB)
Saturation

Fig. 2

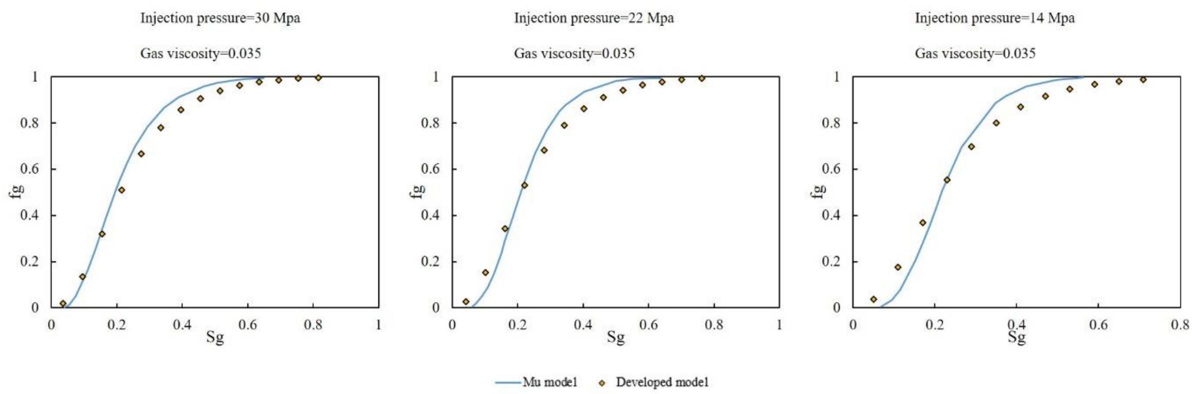
Injection pressure=30 Mpa
Gas viscosity=0.035
Injection pressure=22 Mpa
Gas viscosity=0.035
Injection pressure=14 Mpa
Gas viscosity=0.035
fg
Sg
Mu model
Developed model

Fig.3

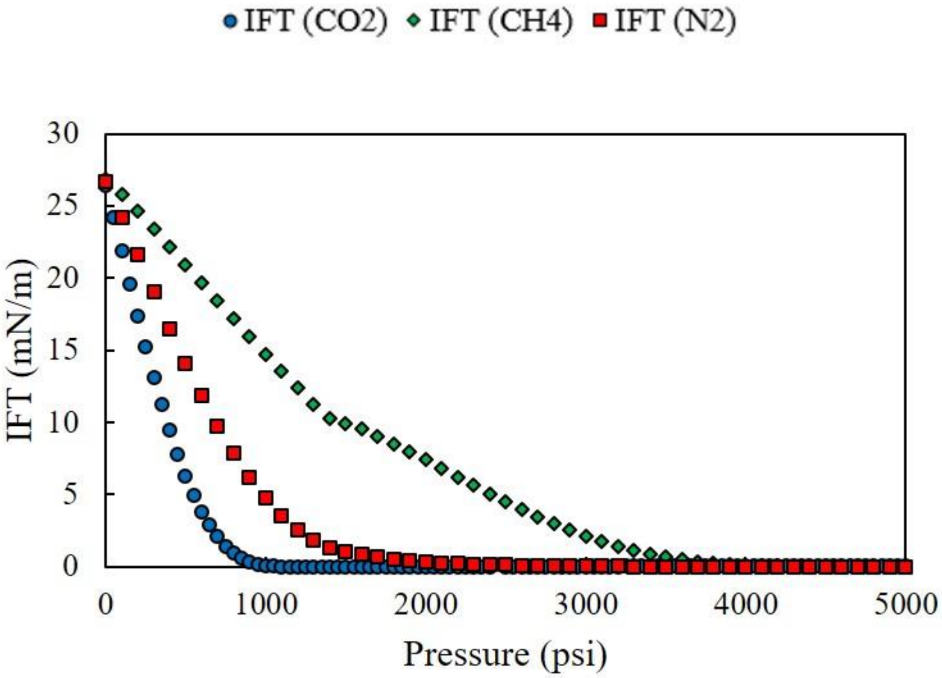

Fig.4

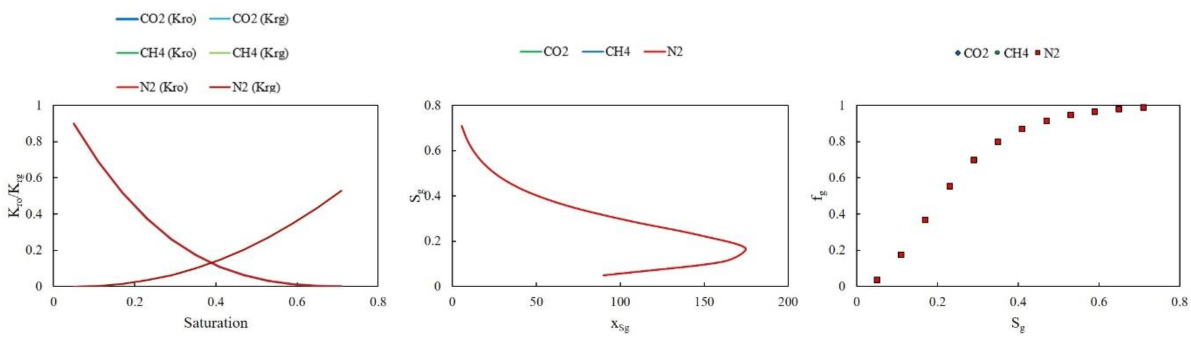

Fig.5

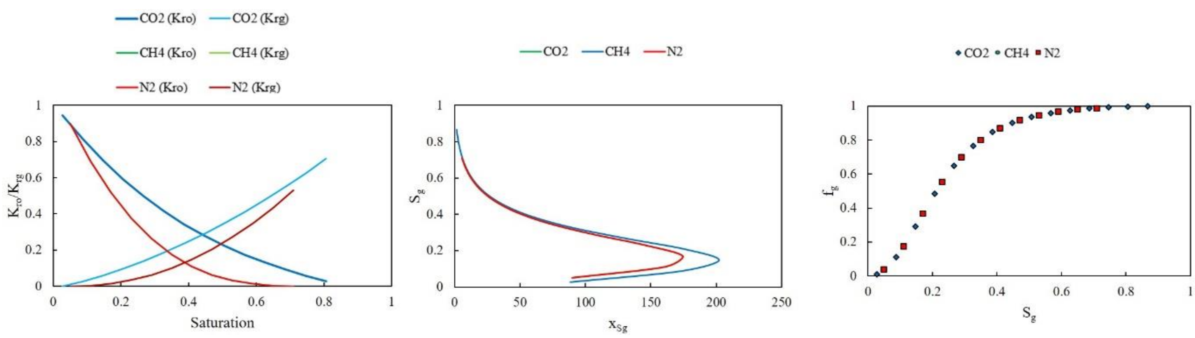

Fig.6

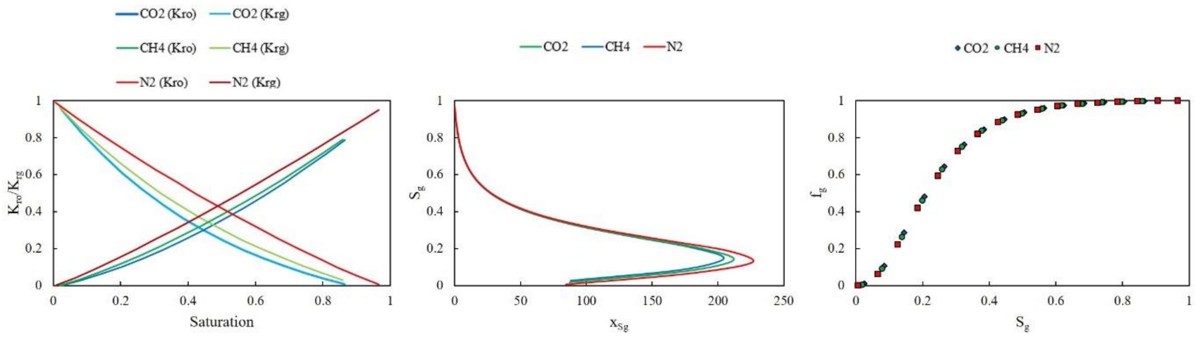

Fig.7

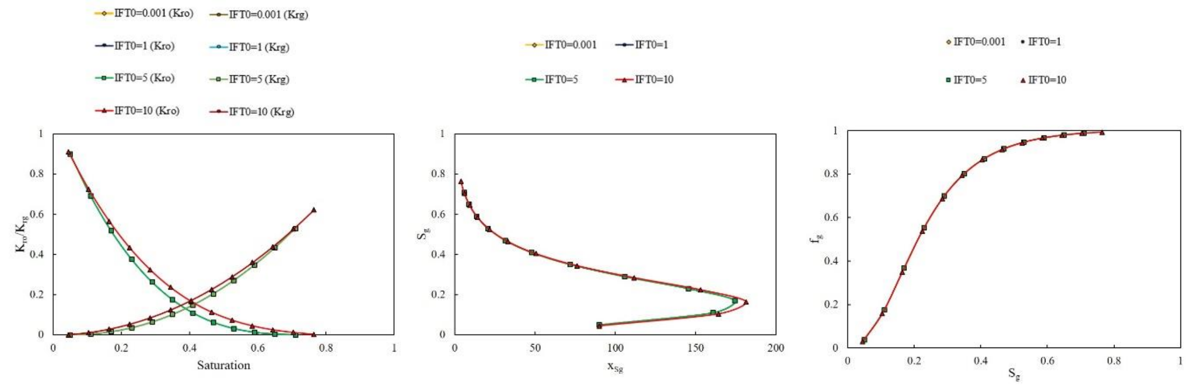

Fig.8

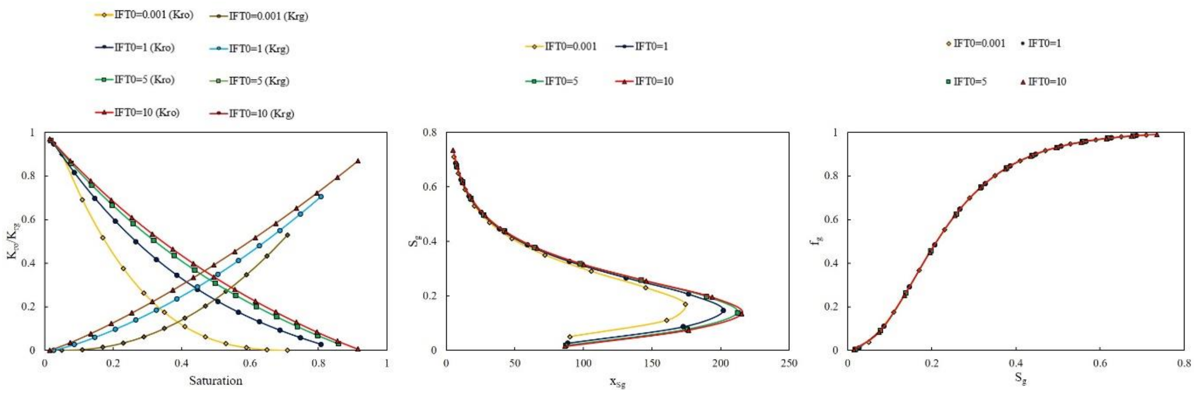

Fig.9

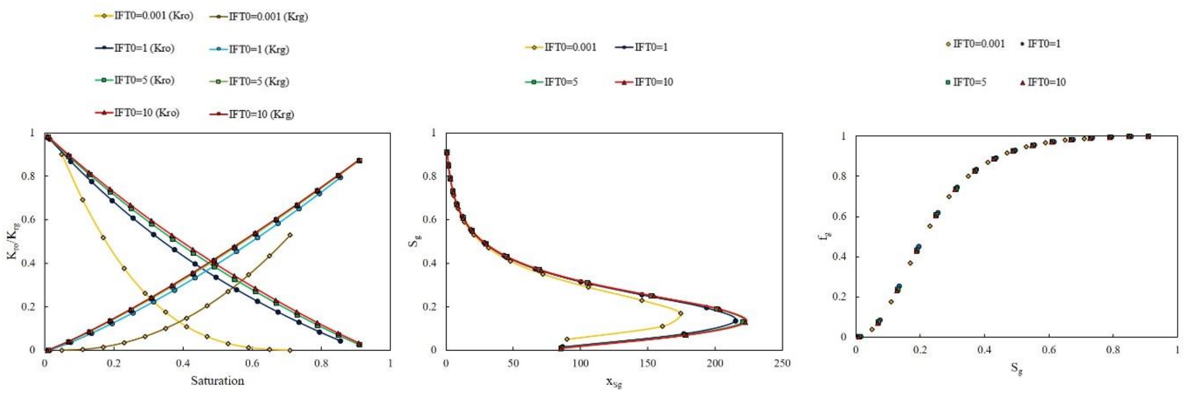

Fig.10

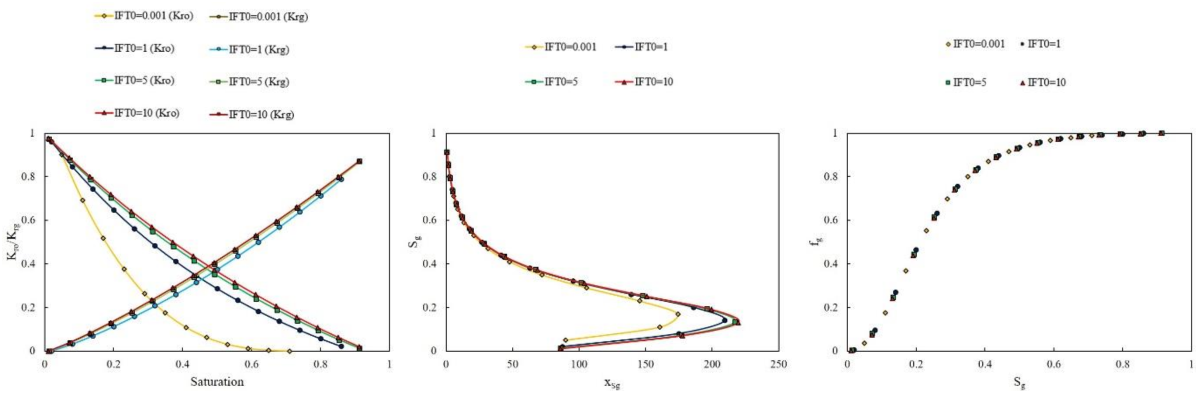

Fig.11

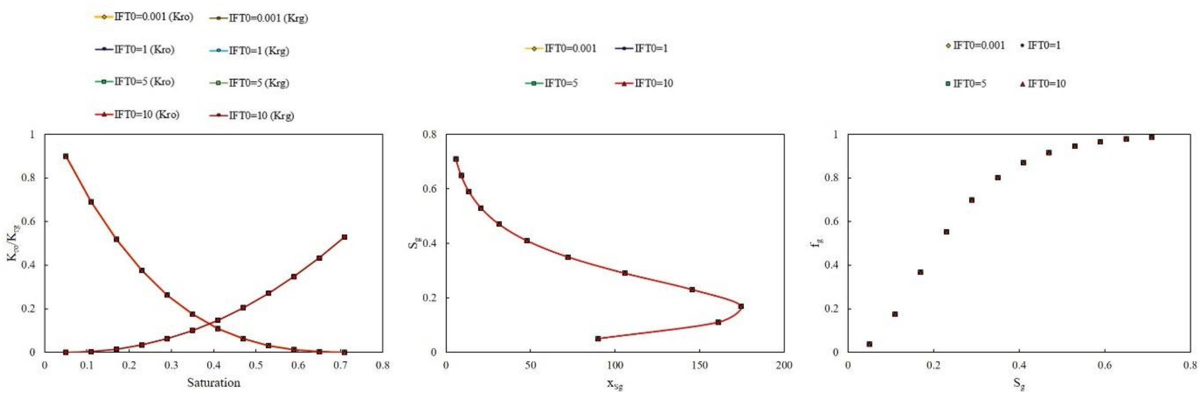

Fig.12

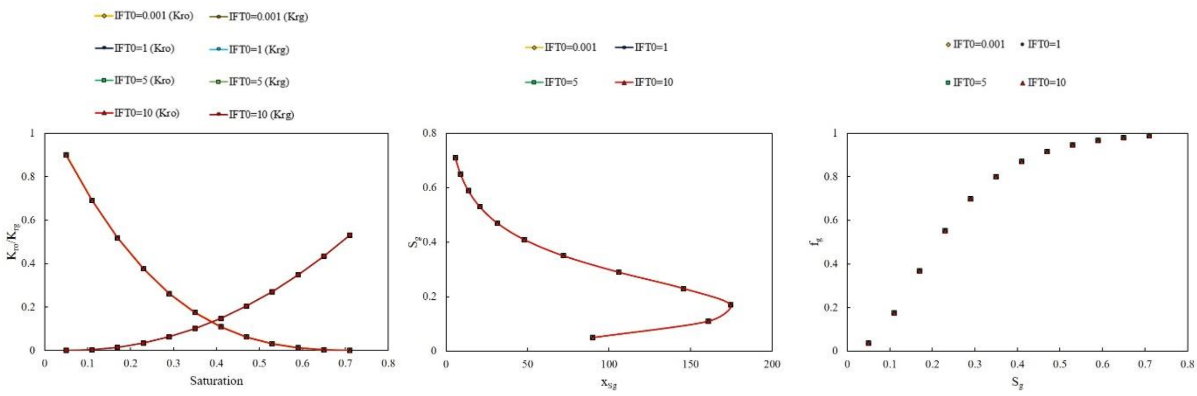

Fig. 13

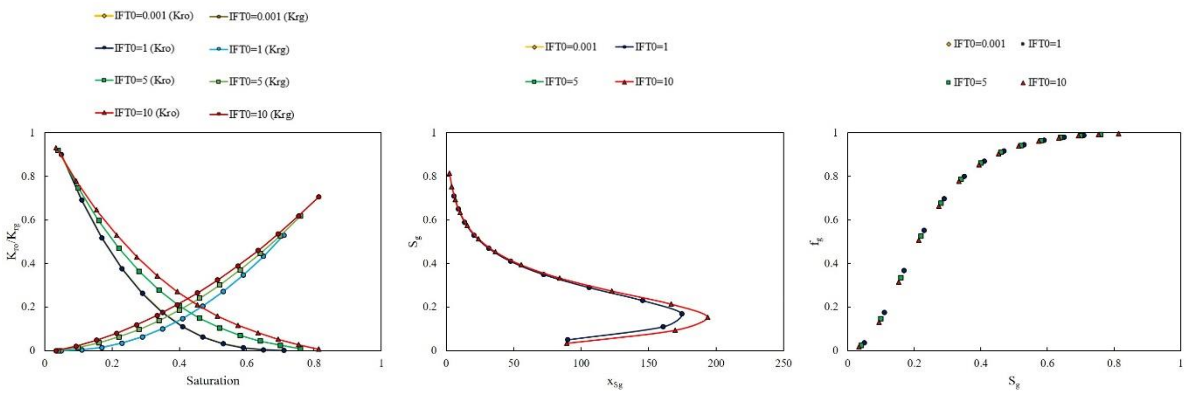

Fig. 14

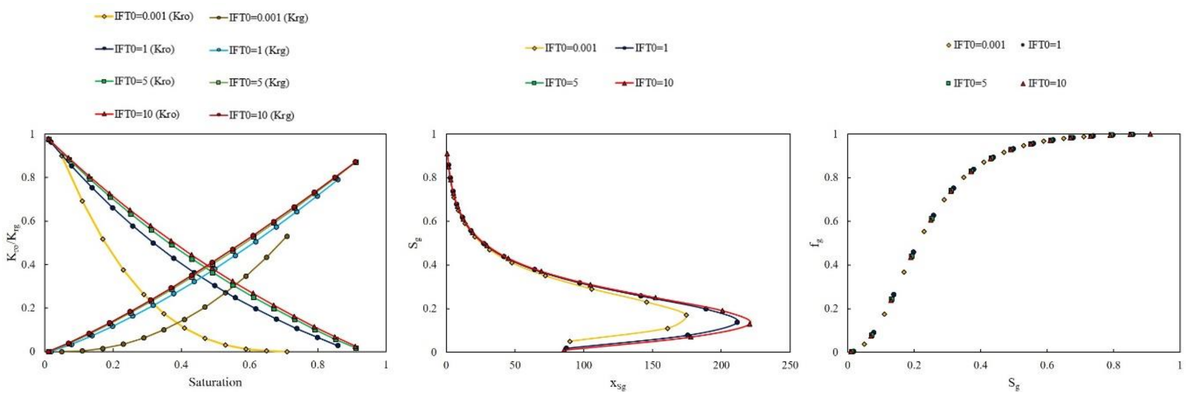

Fig. 15

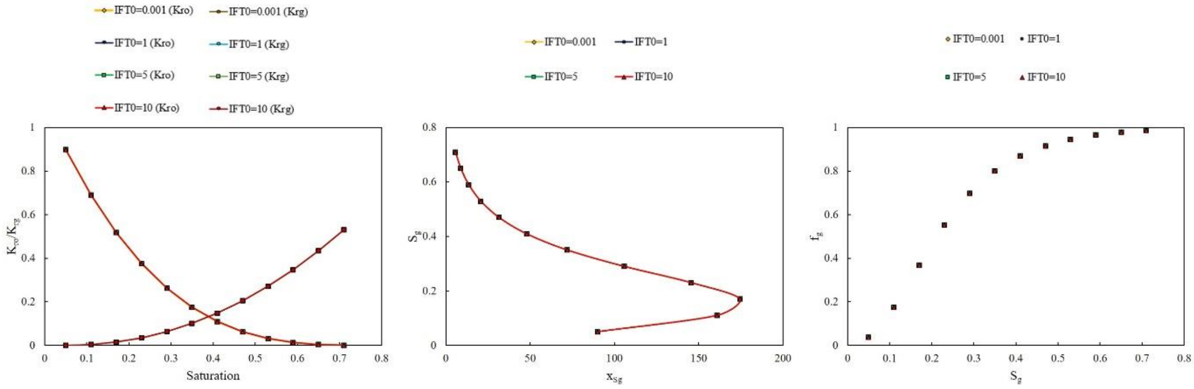

Fig. 16

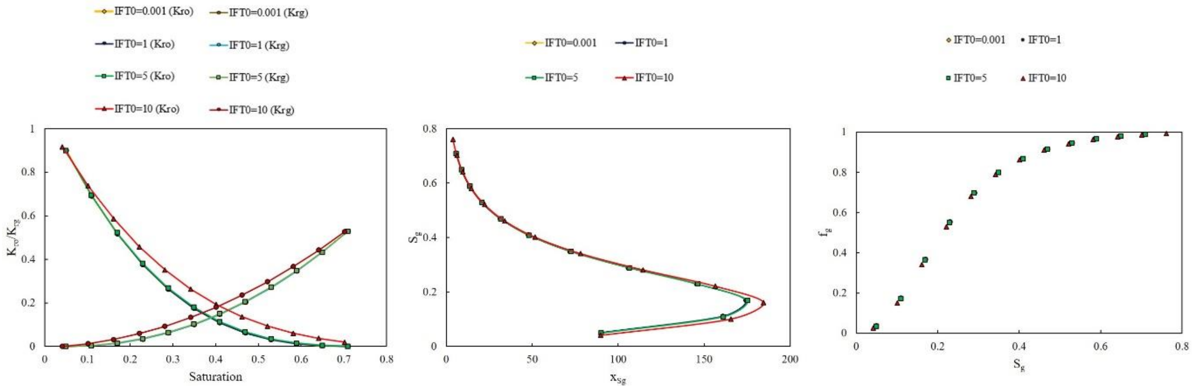

Fig. 17

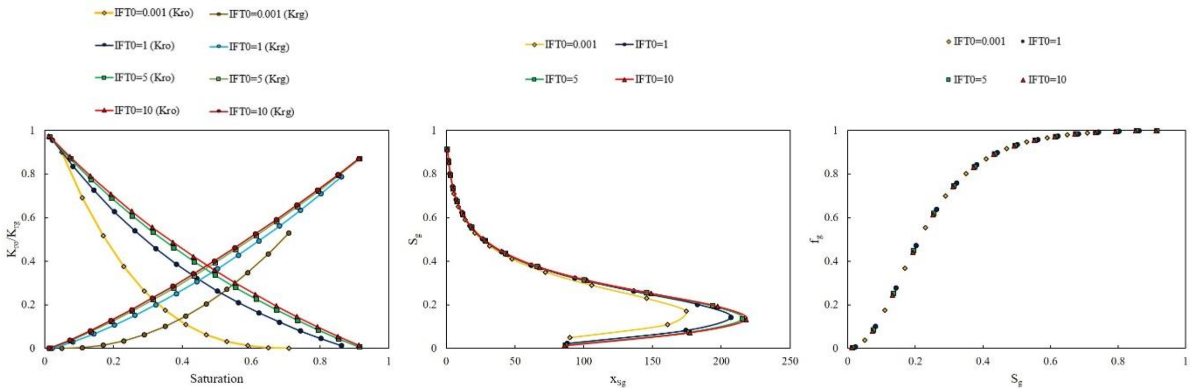

Fig. 18

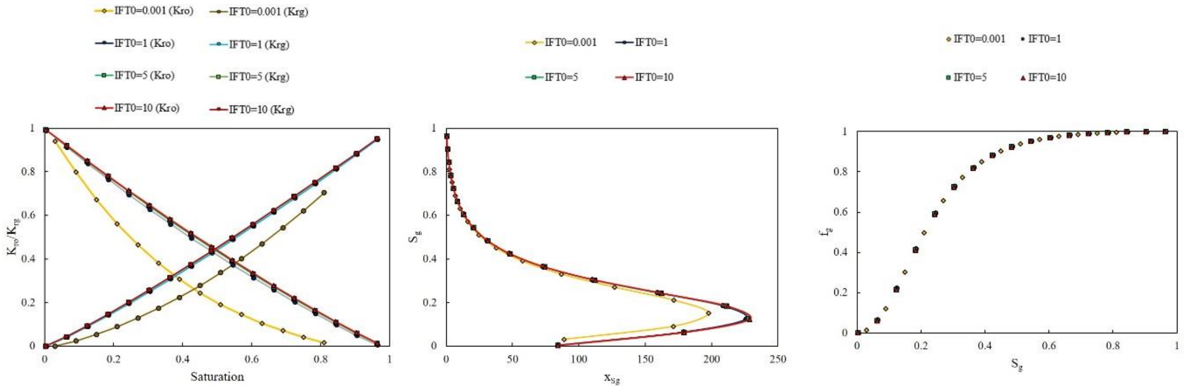

Fig. 19

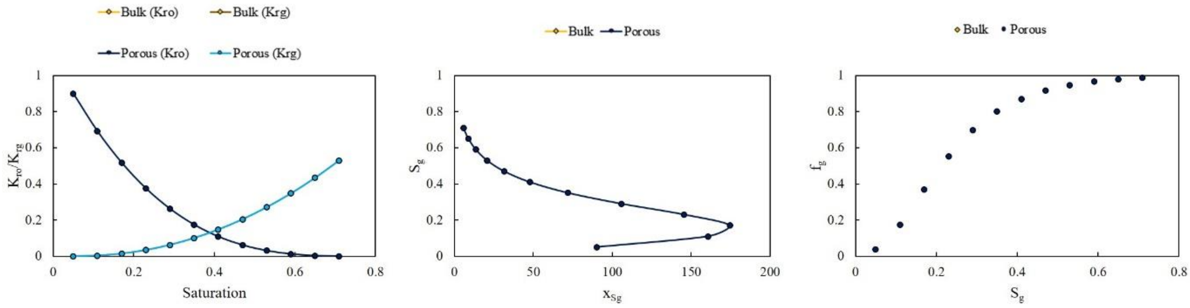

Fig. 20

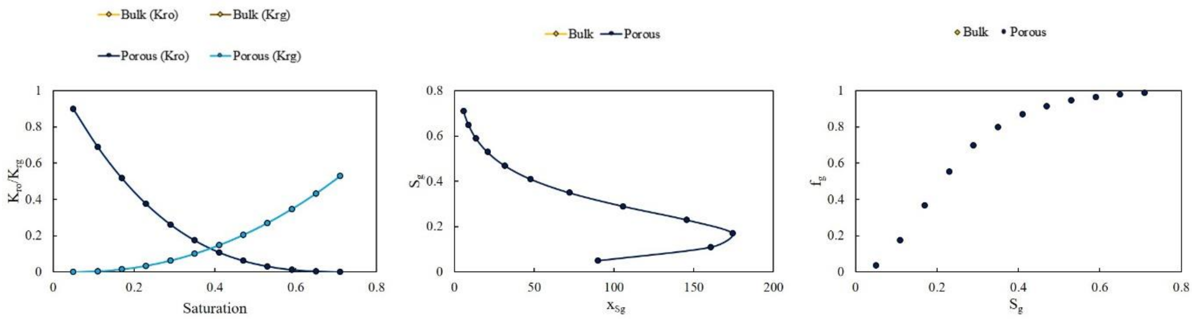

Fig. 21

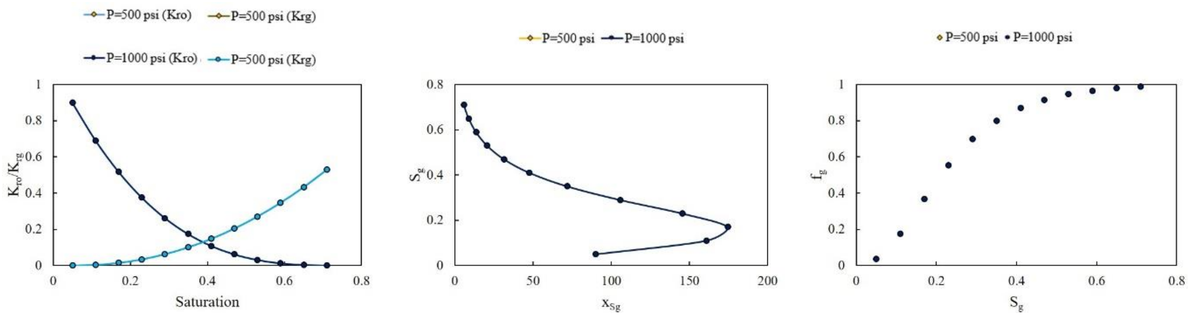

Fig. 22

Authors Biography

Hossein Mehrjoo is a PhD student in Petroleum Engineering at Shahid Bahonar University of Kerman. He holds a BSc degree in Petroleum Engineering from the Islamic Azad University, Bushehr branch. He received his MSc degree in Petroleum Engineering from Shahid Bahonar University of Kerman. His research interests include Acid fracturing, Reactive flow in porous media, EOR, and Machine Learning.

Yousef Kazemzadeh is an assistant professor at Persian Gulf University, Bushehr, Iran. He holds a PhD, MSc, and BSc degrees in Petroleum Engineering from Shiraz University. His current research interests include EOR, Asphaltene Precipitation, Phase behavior of reservoir fluids, and Formation damage.

Ali Safaei is an assistant Professor at the College of Engineering, University of Tehran. He received his PhD degree in Petroleum Engineering from the Shiraz University. His research interests include Wettability Alteration, Sand Production Modeling, Sand Production Control, Imbibition Mathematical modeling, and Miscible gas injection.

Masoud Riazi is a currently associate professor at Petroleum Engineering Department at Nazarbayev University, School of Mining and Geosciences. He holds a PhD in Petroleum Engineering from Heriot-Watt University, a MSc degree in chemical engineering from Tehran University, and a BSc in Petroleum Engineering from Petroleum University of Technology. His current research interests include EOR, Data Analysis, Simulation, Flow at Pore Scale, and CO_2/gas/H_2 storage.